
Frequency Principle: Fourier Analysis Sheds Light on Deep Neural Networks

Zhi-Qin John Xu^{1,2} Yaoyu Zhang^{1,2} Tao Luo³ Yanyang Xiao^{1,2} Zheng Ma³

Abstract

We study the training process of Deep Neural Networks (DNNs) from the Fourier analysis perspective. Our starting point is a Frequency Principle (F-Principle) — DNNs initialized with small parameters often fit target functions from low to high frequencies — which was first proposed by Xu et al. (2018) and Rahaman et al. (2018) on synthetic datasets. In this work, we first show the universality of the F-Principle by demonstrating this phenomenon on high-dimensional benchmark datasets, such as MNIST/CIFAR10. Then, based on experiments, we show that the F-Principle provides insight into both the success and failure of DNNs in different types of problems. Based on the F-Principle, we further propose that DNN can be adopted to accelerate the convergence of low frequencies for scientific computing problems, in which most of the conventional methods (e.g., Jacobi method) exhibit the opposite convergence behavior — faster convergence for higher frequencies. Finally, we prove a theorem for DNNs of one hidden layer as a first step towards a mathematical explanation of the F-Principle. Our work indicates that the F-Principle with Fourier analysis is a promising approach to the study of DNNs because it seems ubiquitous, applicable, and explainable.

1. Introduction

Understanding the training process of Deep Neural Networks (DNNs) is a fundamental problem in the area of deep learning. We found a common implicit bias of gradient-based training of DNNs, that is, a Frequency Principle (F-

¹New York University Abu Dhabi, Abu Dhabi, 129188, United Arab Emirates ²Courant Institute of Mathematical Sciences, 10012, New York University, New York, 10012, NY, United States ³Department of Mathematics, Purdue University, West Lafayette, IN 47907, USA. Correspondence to: Zhi-Qin John Xu <zhiqinxu@nyu.edu>.

Under review of Proceedings of the 36th International Conference on Machine Learning, Long Beach, USA, 2019. Copyright 2019 by the author(s).

Principle):

DNNs initialized with small parameters often fit target functions from low to high frequencies during the training process.

In another word, during the early stage of training, the low-frequencies are fitted and as more iterations of training occur, the high-frequencies are fitted. It has been demonstrated empirically that the F-Principle holds for synthetic low-dimensional problems (Xu et al., 2018; Rahaman et al., 2018). However, its validity in high-dimensional real problems, which is important for the verification of its universality, remains unclear. In this work, we first show that the F-Principle exists in the training process of DNNs of different settings on benchmarks, e.g., MNIST (LeCun, 1998) and CIFAR10 (Krizhevsky et al., 2010). The settings we have considered are i) different DNN architectures, e.g., fully-connected network and convolutional neural network (CNN); ii) different activation functions, e.g., tanh and rectified linear unit (ReLU); iii) different loss functions, e.g., cross entropy, mean squared error (MSE), and loss energy functional in variation problems. These results extend the previous study that mainly focus on synthetic data with mean squared error (Xu et al., 2018; Rahaman et al., 2018), and demonstrate the universality of the F-Principle.

In general, a good characterization of DNN training process should provide insight into the generalization ability of DNNs. As widely observed in experiments, the gradient-based training process biases DNNs towards configurations of different generalization abilities for different problems. In the literature, on the one hand, there are different approaches attempting to mainly explain why the training process often leads to a DNN of good generalization ability even when the number of parameters is much larger than the number of training data (Zhang et al., 2016). For example, generalization error is related to various complexity measures (Bartlett et al., 1999; Bartlett & Mendelson, 2002; Bartlett et al., 2017a;b; Neyshabur et al., 2017; Golowich et al., 2017; Dziugaite & Roy, 2017; Neyshabur et al., 2018; E et al., 2018), local properties (sharpness/flatness) of loss functions at minima (Hochreiter & Schmidhuber, 1995; Keskar et al., 2016; Dinh et al., 2017; Wu et al., 2017), stability of optimization algorithms (Bousquet & Elisseeff, 2002; Xu &

Mannor, 2012; Hardt et al., 2015), and implicit bias of the training process (Neyshabur et al., 2014; Poggio et al., 2018; Soudry et al., 2018; Arpit et al., 2017; Xu et al., 2018). On the other hand, several works focus mainly on the empirical study of the failure of DNNs (Shalev-Shwartz et al., 2017; Nye & Saxe, 2018), in which a well-trained DNN possesses no generalization ability. A well known example is the problem of fitting the parity function (Shalev-Shwartz et al., 2017; Nye & Saxe, 2018). Illustrated by experiments, the F-Principle, which implicates that DNNs prefer low frequencies during fitting the target function, rationalizes different generalization performances of DNNs in both types of problems as follows. For the target functions with dominant low frequencies, e.g., MNIST/CIFAR10, the higher priority of low frequencies naturally results in a faithful fitting of these dominant components. In contrast, for the parity function whose spectrum concentrates at high frequencies, this implicit bias easily leads to artificial low frequencies in the fitting, hence yielding a DNN of poor generalization performance.

In application, how the F-Principle can help devise effective DNN-based approaches to solve scientific computing problems is an important issue (E et al., 2017; Khoo et al., 2017; He et al., 2018; Fan et al., 2018). In this work, based on the F-Principle, we propose that DNN can be adopted to accelerate the convergence of low frequencies for computational problems, in which most of the conventional methods (e.g., Jacobi method) exhibit the opposite convergence behavior — faster convergence for higher frequencies. As a demonstration, for solving Poisson equations, we achieve fast convergence for both low frequencies and high frequencies by combining DNN with conventional Jacobi method.

Finally, as a step towards a mechanistic understanding of the F-Principle, we prove a theorem for DNNs of one hidden layer. Using this theorem, we demonstrate that lower frequencies indeed have higher priorities during the training of DNN. From our analysis, this implicit bias arises from the decaying behavior of power spectrum of commonly used activation functions as a function of frequency. When the weights of a DNN are small, the gradient of the loss function with respect to each parameter is often dominated by low frequencies of the loss function. In conclusion, all our results imply that, among all the functions that can fit the training data, a DNN is implicitly biased following the F-Principle during the training towards a function with more power at low frequencies.

2. F-Principle on benchmarks

Although Xu et al. (2018) and Rahaman et al. (2018) showed the phenomena of the F-Principle on 1-d and 2-d synthetic datasets for the loss function of MSE, there is no empirical study demonstrating such phenomena work for high

dimensional classification problems on real datasets like MNIST/CIFAR10. In this section, we investigate the F-Principle on real datasets. First, we propose a *filtering approach*, inspired by the effectiveness of early stopping in practice, to directly examine the F-Principle for high-dimensional space of real datasets for two commonly used loss functions, that is, MSE and cross entropy. Second, we use a projection method to visualize different convergence speeds of different frequencies of high-dimensional datasets.

2.1. A direct examination of the F-principle in MNIST/CIFAR10 using a filtering approach

In this subsection, we use a filtering approach to directly examine the F-Principle in the training sets of MNIST/CIFAR10. In the following experiments, we consider a training dataset $\{\mathbf{x}_i, \mathbf{y}_i\}_{i=0}^{n-1}$, where n is the size of dataset, $\mathbf{x}_i \in \mathbb{R}^{N_{in}}$ is the input (a one-hot vector indicating the label for the dataset of image classification), N_{in} is the dimension of input ($N_{in} = 784$ for MNIST and $N_{in} = 1024$ for CIFAR10).

A *Gaussian-filtered dataset* $\{\mathbf{x}_i, \mathbf{y}_i^\delta\}_{i=0}^{n-1}$ is used to test the DNN at each training epoch, where

$$\mathbf{y}_i^\delta = \frac{1}{C_i} \sum_{j=0}^{n-1} \mathbf{y}_j \exp(-|\mathbf{x}_i - \mathbf{x}_j|^2 / (2\delta)),$$

$$C_i = \sum_{j=0}^{n-1} \exp(-|\mathbf{x}_i - \mathbf{x}_j|^2 / (2\delta)).$$

For fixed δ , clearly, $\{\mathbf{y}_i^\delta\}$ preserves the low frequency part while losing the high frequency part of $\{\mathbf{y}_i\}$. As δ increases, fewer and fewer high frequencies of $\{\mathbf{y}_i\}$ are preserved in $\{\mathbf{y}_i^\delta\}$.

In the following, we show empirically that the F-Principle is exhibited in the training process of DNNs when applied to real dataset of MNIST/CIFAR10 with the loss function being the widely-used MSE and cross entropy. Among others, we examine two common activation functions: tanh and ReLU, and two types of network structures: fully connected network and convolutional neural network (CNN) for both real datasets, and find that the F-Principle reliably holds. We have examined the F-Principle in different combinations of above settings. For illustration, for MNIST, we use a fully connected tanh-DNN with widths 784-400-200-10 and MSE loss; for CIFAR10, we use cross-entropy loss and a ReLU-CNN, which consists of one convolution layer of $3 \times 3 \times 32$, a max pooling of 2×2 , one convolution layer of $3 \times 3 \times 64$, a max pooling of 2×2 , followed by a fully connected DNN with widths 400-10 and the output layer of the network is equipped with a softmax.

As an example, results of each dataset for one δ are shown in Fig. 1(a). By the F-Principle, at the early stage of training,

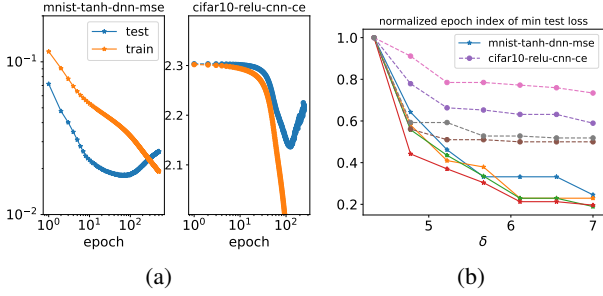


Figure 1. F-Principle in MNIST and CIFAR10. (a) Loss functions against training epoch. $\delta = 7$ and 4.3 for MNIST (left) and CIFAR10 (right), respectively. (b) The turning epoch, normalized by the maximum turning epoch number of each trial, is plotted against filter width δ . Solid and dashed curves are for MNIST and CIFAR10, respectively. Each curve is for one trial. The learning rate for MNIST and CIFAR10 is 0.015 and 0.003, respectively. The networks are trained by Adam optimizer (Kingma & Ba, 2014) with batch size 10000.

DNN captures the low frequency part of $\{y_i\}$. Thus, using $\{y_i^\delta\}$ as the test data, the test loss keeps decreasing. At a later training stage, by the F-Principle, DNN starts to fit the high frequency part of $\{y_i\}$, leading to an increasing test loss. At the *turning epoch of training*, at which the test loss function attains its minimum, indicating that the high frequency part of $\{y_i^\delta\}$ starts to dominate the training of DNN over the low frequency part. Therefore, after the turning point, we observe a decreasing training loss whereas an increasing test loss as shown in Fig. 1(a). As δ increases, by the F-Principle, one will expect that the turning epoch comes earlier because $\{y_i^\delta\}$ preserves components of lower frequencies which are captured at an earlier stage.

We scan δ for 4 trials of training with different initializations. In each trial, for different δ 's, all other settings are *exactly the same (including initialization)*. As shown in Fig. 1(b), the turning epoch decreases with δ . Based on above results, for MNIST/CIFAR10, DNN captures higher frequencies at later training epochs following the F-Principle. We also remark that, based on above results on cross-entropy loss, the F-Principle is not limited to MSE loss, which possesses a natural Fourier domain interpretation by the Parseval's theorem as illustrated in Xu et al. (2018) and Rahaman et al. (2018). Note that the above results holds for optimization methods of both gradient descent and stochastic gradient descent.

2.2. Visualization of convergence speed at Fourier space using projection method

To further illustrate the F-principle in real datasets of MNIST and CIFAR10, we visualize the different conver-

gence speeds of different frequencies in the following.

For a dataset $\{\mathbf{x}_j, y_j\}_{j=0}^{n-1}$, for illustration, we consider one dimension of output, denoted by $y_j \in \mathbb{R}$. The high dimensional discrete non-uniform Fourier transform of $\{\mathbf{x}_j, y_j\}_{j=0}^{n-1}$ is $\hat{y}_{\mathbf{k}} = \frac{1}{n} \sum_{j=0}^{n-1} y_j \exp(-i2\pi \mathbf{k} \cdot \mathbf{x}_j)$. The number of all possible \mathbf{k} grows exponentially on dimension N_{in} . Here, for illustration, we only consider one direction of \mathbf{k} in the Fourier space, i.e., $\mathbf{k} = k\mathbf{p}_1$, where $k = |\mathbf{k}|$ and \mathbf{p}_1 is a chosen and fixed unit vector. Then, we have $\hat{y}_k = \frac{1}{n} \sum_{j=0}^{n-1} y_j \exp(-i2\pi k \mathbf{p}_1 \cdot \mathbf{x}_j) = \frac{1}{n} \sum_{j=0}^{n-1} y_j \exp(-i2\pi (\mathbf{p}_1 \cdot \mathbf{x}_j) k)$, which is essentially the 1-d Fourier transform of $\{x_{\mathbf{p}_1, j}, y_j\}_{j=0}^{n-1}$, where $x_{\mathbf{p}_1, j} = \mathbf{p}_1 \cdot \mathbf{x}_j$ is the projection of \mathbf{x}_j on the direction \mathbf{p}_1 (Bracewell & Bracewell, 1986).

For each training dataset, \mathbf{p}_1 is chosen as the first principle component of the input space. To examine the convergence behavior of different frequency components during the training, we compute the relative difference of certain DNN output dimension $\{\Upsilon_j\}_{j=0}^{n-1}$ and $\{y_j\}_{j=0}^{n-1}$ for a range of k 's in the frequency domain at each recording step, that is,

$$\Delta_F(k) = \frac{|\hat{\Upsilon}_k - \hat{y}_k|}{|\hat{y}_k|}, \quad (1)$$

where \hat{y}_k and $\hat{\Upsilon}_k$ are 1-d Fourier transforms of $\{y_j\}_{j=0}^{n-1}$ and $\{\Upsilon_j\}_{j=0}^{n-1}$, respectively, along the direction \mathbf{p}_1 and the projected data points of $\{x_{\mathbf{p}_1, j}\}_{j=0}^{n-1}$.

In the following, we show empirically that the F-Principle is exhibited in the selected direction during the training process of DNNs when applied to real dataset of MNIST/CIFAR10 with cross-entropy loss. As an example, for MNIST dataset, the training process of a tanh-DNN with widths 784-400-200-10 is shown in Fig. 2(a) and 2(b). For CIFAR10 dataset, results are shown in Fig. 2(c) and 2(d) of a ReLU-CNN, which consists of one convolution layer of $3 \times 3 \times 64$, a max pooling of 2×2 , one convolution layer of $3 \times 3 \times 128$, a max pooling of 2×2 , followed by a fully connected DNN with widths 800-400-400-400-10. For both cases, the output layer of the network is equipped with a softmax. The network output is a 10-d vector. For illustration, we consider one of the 10-d outputs in each case. Using non-uniform Fourier transform, as shown in Fig. 2(a) and 2(c), low frequencies dominate in both real datasets. During the training, the evolution of relative errors of certain selected frequencies (marked by black squares in Fig. 2(a) and 2(c)) is shown in Fig. 2(b) and 2(d). One can easily observe that DNNs capture low frequencies first and gradually capture higher frequencies. Clearly, this behavior is consistent with the F-Principle discovered in Xu et al. (2018) using synthetic datasets. For other components of the output vector and other directions of \mathbf{p} , similar phenomena are also observed.

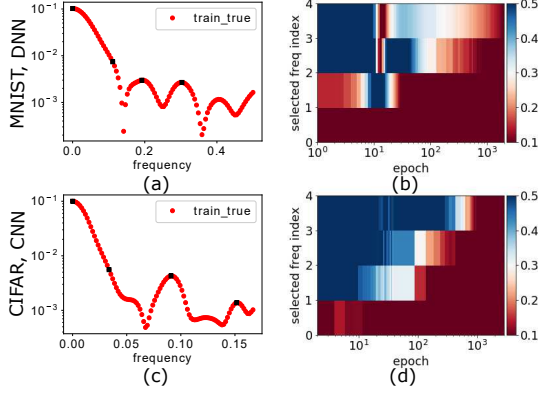


Figure 2. Projection method for examining F-Principle in DNN training with cross entropy loss by Adam optimizer (Kingma & Ba, 2014). The first row is for MNIST with a tanh-DNN. The learning rate is 0.001 with batch size 10000. After training, the training accuracy is 0.951 and test accuracy is 0.963. The amplitude of the Fourier coefficient with respect to the fourth output component at each frequency is shown in (a), in which the red dots are computed using the training data. Selected frequencies are marked by black squares. (b) $\Delta_F(k)$ at different training epochs for the selected frequencies. The second row is for CIFAR10 dataset. We use a ReLU network of a CNN followed by a fully connected DNN. The learning rate is 0.003 with batch size 512. (c) and (d) are the results with respect to the ninth output component. After training, the training accuracy is 0.98 and test accuracy is 0.72.

3. Understanding different generalization performances of DNN through F-Principle

It has been widely observed that DNNs often generalize well in a variety of real problems, e.g., image classification (Zhang et al., 2016). Meanwhile, it has been shown that DNNs have no generalization ability in fitting the parity function (Shalev-Shwartz et al., 2017; Nye & Saxe, 2018). Understanding the differences between above two types of problems, i.e., good and bad generalization performance of DNN, is a critical issue in application. In this section, we provide a qualitative characterization of differences between these two types of problems through *Fourier analysis* and then use the *F-Principle* to provide insight into how different characteristics in Fourier domain result in different generalization performances of DNNs.

For MNIST/CIFAR10, we have examined $\hat{y}_{\text{total},\mathbf{k}} = \frac{1}{n_{\text{total}}} \sum_{j=0}^{n_{\text{total}}-1} y_j \exp(-i2\pi\mathbf{k} \cdot \mathbf{x}_j)$, where $\{\mathbf{x}_j, y_j\}_{j=0}^{n_{\text{total}}-1}$ consists of both the training and test datasets with certain selected output component, at a variety of different directions of \mathbf{k} in the Fourier space. We find that $\hat{y}_{\text{total},\mathbf{k}}$ concentrates on the low frequencies along those examined directions. As an illustration, $\hat{y}_{\text{total},\mathbf{k}}$'s along the direction of the first

principle component are shown by green lines in Fig. 3(a) and 3(b) for MNIST/CIFAR10, respectively. When only the training dataset is used, $\hat{y}_{\text{train},\mathbf{k}}$ well overlaps with $\hat{y}_{\text{total},\mathbf{k}}$ at the dominant low frequencies.

For the parity function $f(\mathbf{x}) = \prod_j x_j$ defined on $\Omega = \{-1, 1\}^{N_{\text{in}}}$, its Fourier transform is $\hat{f}(\mathbf{k}) = \frac{1}{2^{N_{\text{in}}}} \sum_{\mathbf{x} \in \Omega} \prod_j x_j e^{-i2\pi\mathbf{k} \cdot \mathbf{x}} = (-i)^{N_{\text{in}}} \prod_j \sin 2\pi k_j$. Clearly, for $\mathbf{k} \in [-\frac{1}{4}, \frac{1}{4}]^{N_{\text{in}}}$, the power of the parity function concentrates at $\mathbf{k} \in \{-\frac{1}{4}, \frac{1}{4}\}^{N_{\text{in}}}$ and vanishes as $\mathbf{k} \rightarrow \mathbf{0}$, as illustrated in Fig. 3(c) for the direction of $\mathbf{1}_{N_{\text{in}}}$. Given a randomly sampled training dataset $S \subset \Omega$ with s points, the nonuniform Fourier transform on S is computed as $\hat{f}_S(\mathbf{k}) = \frac{1}{s} \sum_{\mathbf{x} \in S} \prod_j x_j e^{-i2\pi\mathbf{k} \cdot \mathbf{x}}$. As shown in Fig. 3(c), $\hat{f}(\mathbf{k})$ and $\hat{f}_S(\mathbf{k})$ significantly differ at low frequencies.

By experiments, the generalization ability of DNNs can be well reflected by the Fourier analysis. For the MNIST/CIFAR10, we observed the Fourier transform of the output of a well-trained DNN on $\{\mathbf{x}_j\}_{j=0}^{n_{\text{total}}-1}$ faithfully recovers the dominant low frequencies, as illustrated in Fig. 3(a) and 3(b), respectively, indicating a good generalization performance as observed in experiments. However, for the parity function, we observed that the Fourier transform of the output of a well-trained DNN on $\{\mathbf{x}_j\}_{j \in S}$ significantly deviates from $\hat{f}(\mathbf{k})$ at almost all frequencies, as illustrated in Fig. 3(c), indicating a bad generalization performance as observed in experiments.

The F-Principle implicates that, among all the functions that can fit the training data, a DNN is implicitly biased during the training towards a function with more power at low frequencies. If the target function has significant high frequency components, insufficient training samples will lead to artificial low frequency components in the Fourier transform of training dataset, as shown in Fig. 3(c), due to aliasing. Based on the F-Principle, as demonstrated in Fig. 3(c), these artificial low frequency components will be first captured to explain the training samples, whereas the high frequency components will be compromised by DNN. For MNIST/CIFAR10, since the power of high frequencies is much smaller than that of low frequencies, artificial low frequency components caused by aliasing can be neglected. However, for the parity function, its power concentrates at high frequencies. Therefore, the artificial low frequency components are very significant and will be falsely captured by the DNN during the training. To conclude, the distribution of power in Fourier domain of above two types of problems exhibits significant differences, which result in different generalization performances of DNNs according to the F-Principle.

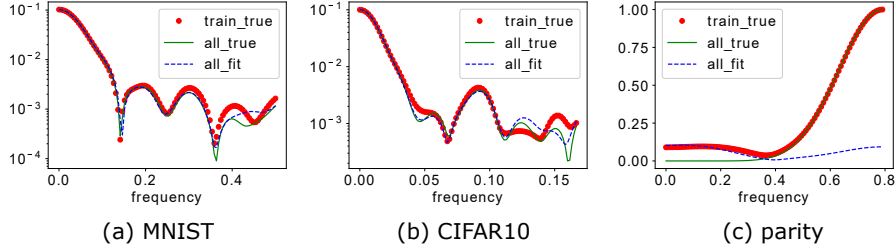


Figure 3. Fourier analysis of DNN output with different generalization ability. The plot is the amplitude of the Fourier coefficient against frequency k . The red dots are for the training dataset, the green line is for the whole dataset, and the blue dashed line is for an output of well-trained DNN on the input of the whole dataset. The settings of (a) and (b) are the same as the ones in Fig. 2. \mathbf{p}_1 is chosen as the normalized first principle component of the training dataset for (a) and (b). The setting for (c) is as follows. The target function is the parity function with input dimension 10. The training dataset is 200 randomly selected points, and the whole dataset is all 2^{10} points. For illustration, we choose the projection direction $\mathbf{p}_1 = 1_{10}$. We use a tanh-DNN with widths 10-500-100-1, learning rate 0.0005 under full batch-size training by Adam optimizer (Kingma & Ba, 2014). The parameters of the DNN are initialized by a Gaussian distribution with mean 0 and standard deviation 0.05.

4. An application of F-Principle: solving Poisson’s equation

Recently, DNN-based approaches have been actively explored for a variety of scientific computing problems, e.g., solving high-dimensional partial differential equations (E et al., 2017; Khoo et al., 2017; He et al., 2018; Fan et al., 2018) and molecular dynamics (MD) simulations (Han et al., 2017). However, the behaviors of DNNs applied to these problems are not well-understood. To facilitate the designs and applications of DNN-based schemes, it is important to characterize the differences between DNNs and conventional numerical schemes on various scientific computing problems. In this section, focusing on solving Poisson’s equation, which has broad utility in mechanical engineering and theoretical physics (Evans, 2010), we investigate the behaviors of a DNN-based solver and the Jacobi method during the training/iteration from the Fourier analysis perspective.

Consider a 1-d Poisson’s equation (Evans, 2010):

$$-\Delta u(x) = g(x), \quad x \in \Omega = (-1, 1), \quad (2)$$

$$u(-1) = u(1) = 0. \quad (3)$$

In E & Yu (2018), a DNN-based scheme is proposed by considering the following loss energy functional (loss function),

$$I(u) = \int_{\Omega} \left(\frac{1}{2} |\nabla_x u(x)|^2 - g(x)u(x) \right) dx + \beta \int_{\partial\Omega} u(x)^2 ds. \quad (4)$$

By variational principle (Evans, 2010), minimizing the first term in $I(u)$ is equivalent to solving the Poisson’s equation. The second term in $I(u)$ is a penalty, with constant β , arising from the Dirichlet boundary condition (3). In Fig. 4, we consider the example of $g(x) = \sin(x) +$

$4 \sin(4x) - 8 \sin(8x) + 16 \sin(24x)$ with analytical solution $u_{\text{ref}}(x) = g_0(x) + c_1 x + c_0$, where $g_0 = \sin(x) + \sin(4x)/4 - \sin(8x)/8 + \sin(24x)/36$, $c_1 = (g_0(-1) - g_0(1))/2$ and $c_0 = -(g_0(-1) + g_0(1))/2$. We use a DNN with widths 1-4000-500-400-1 for solving Eq. (4). Here, we use the DNN output, $\Upsilon(x; \Theta)$, to fit $u_{\text{ref}}(x)$ (Fig. 4(a)). The training samples $\{x_j\}_{j=0}^n$ are evenly spaced with grid size h in $[0, 1]$ with sample size 1001. In each training step, we compute $\Upsilon(x_i; \Theta)$ for $i = 0, 1, 2, \dots, n$. The empirical loss is

$$I_{\text{emp}} = \sum_{i=1}^{n-1} \left(\frac{1}{2} |\nabla_x \Upsilon(x_i)|^2 - g(x_i) \Upsilon(x_i) \right) h + \beta (\Upsilon(x_0)^2 + \Upsilon(x_n)^2).$$

The partial derivative of I_{emp} with respect to a parameter $\theta \in \Theta$, $\frac{\partial I_{\text{emp}}}{\partial \theta}$, is then used for gradient descent tuning. After training, the DNN output well matches the analytical solution u_{ref} . Focusing on the convergence of three peaks (inset of Fig. 4(a)) in the Fourier transform of u_{ref} , as shown in Fig. 4(b), low frequencies converge faster than high frequencies as predicted by the F-Principle.

For comparison, we also show the iterative process of the Jacobi method, one of the commonly used methods, to solve problem (2). With $[-1, 1]$ uniformly discretized, the Poisson’s equation can be solved by the central difference scheme, resulting in a linear system $\mathbf{A}\mathbf{u} = \mathbf{g}$, where \mathbf{A} , \mathbf{g} and \mathbf{u} can be found in Appendix A. The Jacobi method can then be applied to solve this linear system. theoretically, high frequencies which correspond to small eigenvalues of \mathbf{A} converge faster in the Jacobi method (see Appendix A), as illustrated in Fig. 4(c).

Based on the above results, we further propose that DNN can be combined with conventional numerical schemes to accelerate the convergence of low frequencies for a variety of computational problems. As a demonstration, we solve the Poisson’s equation by combining DNN and Jacobi

method. First, we solve the Poisson's equation in Eq. (2) by DNN with M optimization steps (or epochs), which is chosen carefully, to get a good initial guess in the sense that this solution has already damped out the low frequencies (big eigenvalues) part. Then, we use the Jacobi method with the new initial data for the further iterations. We use $|\Upsilon - u_{\text{ref}}|_{\infty} \triangleq \max_x |\Upsilon(x) - u_{\text{ref}}(x)|$ to quantify the learning result. As shown by green stars in Fig. 4(d), $|\Upsilon - u_{\text{ref}}|_{\infty}$ fluctuates after some running time using DNN only. Dashed lines indicate the evolution of the Jacobi method with initial data set to the DNN output at the corresponding steps. If M is too small (stop too early) (left dashed line), it would still take long time to converge to a small error, because low frequencies are not converged, yet. If M is too big (stop too late) (right dashed line), much time would be wasted for the slow convergence of high frequencies by DNN. A proper choice of M is indicated by the initial point of orange dashed line, in which low frequencies are quickly captured by the DNN, followed by fast convergence of high frequencies of the Jacobi method. This example illustrates a cautionary tale that, although DNNs has clear advantage, using DNNs alone may not be the best option because of its limitation of slow convergence at high frequencies. Taking advantage of both DNNs and conventional methods to design faster schemes could be a promising direction in scientific computing problems.

5. F-Principle and initialization of DNN

In this section, we study the F-Principle about its dependence on the initialization of the weights. We also provide a theorem to explain the result.

5.1. Experiment

We train a tanh-DNN, denoted by $\Upsilon(x)$, with widths 1-8000-1 to fit the target function $f(x) = \sin(x) + \sin(3x) + \sin(5x)$ in Fig. 5(a). In two experiments, the parameters of the DNN are initialized differently by a Gaussian distribution with mean 0 and standard deviation 0.1 (small initial parameters) or 25 (large initial parameters). On evenly spaced grids $\{x_j\}_{j=0}^{n-1}$ of the input of training samples, the discrete Fourier transform (DFT) of $f(x)$ or $\Upsilon(x)$ is computed by $\hat{f}(k) = \frac{1}{n} \sum_{j=0}^{n-1} f(x_j) e^{-2\pi i j k / n}$ and $\hat{\Upsilon}(k) = \frac{1}{n} \sum_{j=0}^{n-1} \Upsilon(x_j) e^{-2\pi i j k / n}$.

We consider the three important frequencies (black dots at the inset in Fig. 5(a)) of the target function. For the case of small initial parameters, as shown in Fig. 5(b), the DNN converges, marching from low to high frequency. For the case of large initial parameters, the convergence behavior of the three important frequencies do not exhibit a clear order from low to high frequencies (Fig. 5(c)). Taken together,

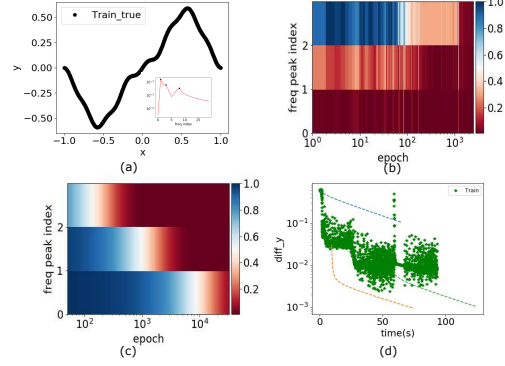


Figure 4. Fourier analysis of the Poisson's equation (2) with $g(x) = \sin(x) + 4\sin(4x) - 8\sin(8x) + 16\sin(24x)$. (a) The analytical solution $u_{\text{ref}}(x)$. Inset: $|\hat{u}_{\text{ref}}(k)|$ (red solid line) as a function of frequency. The peaks of frequencies are marked with black dots. (b,c) $\Delta_F(k)$ computed on the inputs of training data at different epochs for the selected frequencies of DNN (b) and Jacobi method (c). (d) $|\Upsilon - u_{\text{ref}}|_{\infty}$ at different running time. Green stars indicate $|\Upsilon - u_{\text{ref}}|_{\infty}$ using DNN alone. The dashed lines indicate $|\Upsilon - u_{\text{ref}}|_{\infty}$ for the Jacobi method with different colors indicating initialization at different timing of DNN training. The samples are evenly spaced in $[0, 1]$ with sample size 1001. We use a DNN with widths 1-4000-500-400-1 and full batch training by Adam optimizer (Kingma & Ba, 2014). The learning rate is 0.0005. β is 10. The parameters of the DNN are initialized following a Gaussian distribution with mean 0 and standard deviation 0.02.

the magnitude of the weight significantly affects the DNN training process.

5.2. Theorem

In this section, we will develop a theorem focusing on DNNs of one hidden layer with the loss of MSE to provide insight into the key mechanism underlying the F-Principle as well as how small initialization could benefit the F-Principle. The activation function we consider is a tanh function $\sigma(x)$:

$$\sigma(x) = \tanh(x) = \frac{e^x - e^{-x}}{e^x + e^{-x}}, \quad x \in \mathbb{R}.$$

For a DNN of one hidden layer with N nodes, 1-d input x and 1-d output:

$$\Upsilon(x) = \sum_{i=1}^N a_i \sigma(w_i x + b_i), \quad a_i, w_i, b_i \in \mathbb{R}, \quad (5)$$

where w_i , a_i , and b_i are called *parameters*, in particular, w_i and a_i are called *weights*, and b_i is also known as a *bias*. In the sequel, we will also use the notation $\Theta = \{\Theta_{ij}\}$ with $\Theta_{i1} = a_i$, $\Theta_{i2} = w_i$, and $\Theta_{i3} = b_i$, $i = 1, \dots, N$. Note that $\hat{\sigma}(k) = -\frac{i\pi}{\sinh(\pi k/2)}$ where the Fourier transformation and its

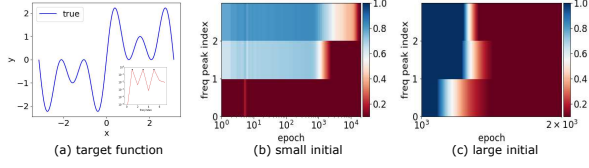


Figure 5. Fourier analysis of the training process of a DNN with different magnitudes of initial parameters for fitting $f(x) = \sin(x) + \sin(3x) + \sin(5x)$. The training samples are evenly sampled from $[-3.14, 3.14]$ with sample size 201. (a) The target function $f(x)$. Inset in (a): $|\hat{f}(k)|$ computed from training samples. (b) and (c) are $\Delta_F(k)$ computed on the inputs of training data at different epochs at the selected frequencies indicated by black dots in the inset of (a). The parameters of the DNN is initialized by a Gaussian distribution with mean 0 and standard deviation 0.1 (small initial parameters) for (b) and 25 (large initial parameters) for (d). We use a tanh-DNN with widths 1-8000-1 with full batch training. The learning rate is 0.0002. The DNN is trained by Adam optimizer (Kingma & Ba, 2014) with the MSE loss function.

inverse transformation are defined as follows:

$$\hat{f}(k) = \int_{-\infty}^{+\infty} f(x)e^{-ikx} dx, \quad f(x) = 2\pi \int_{-\infty}^{+\infty} \hat{f}(k)e^{ikx} dk.$$

The Fourier transform of $\sigma(w_i x + b_i)$ with $w_i, b_i \in \mathbb{R}$, $i = 1, \dots, N$ reads as

$$\widehat{\sigma(w_i \cdot + b_i)}(k) = \frac{2\pi i}{|w_i|} \exp\left(\frac{ib_i k}{w_i}\right) \frac{1}{\exp(-\frac{\pi k}{2w_i}) - \exp(\frac{\pi k}{2w_i})}. \quad (6)$$

Thus

$$\hat{Y}(k) = \sum_{i=1}^N \frac{2\pi a_i i}{|w_i|} \exp\left(\frac{ib_i k}{w_i}\right) \frac{1}{\exp(-\frac{\pi k}{2w_i}) - \exp(\frac{\pi k}{2w_i})}. \quad (7)$$

We define the amplitude deviation between DNN output and the target function $f(x)$ at frequency k as

$$D(k) \triangleq \hat{Y}(k) - \hat{f}(k).$$

Write $D(k)$ as $D(k) = A(k)e^{i\phi(k)}$, where $A(k) \in [0, +\infty)$ and $\phi(k) \in \mathbb{R}$ are the amplitude and phase of $D(k)$, respectively. The loss at frequency k is $L(k) = \frac{1}{2}|D(k)|^2$, where $|\cdot|$ denotes the norm of a complex number. The total loss function is defined as: $L = \int_{-\infty}^{+\infty} L(k) dk$. Note that according to the Parseval's theorem, this loss function in the Fourier domain is equal to the commonly used loss of mean squared error, that is, $L = \int_{-\infty}^{+\infty} \frac{1}{2}(\Upsilon(x) - f(x))^2 dx$. For readers' reference, we list the partial derivatives of $L(k)$ with respect to param-

eters

$$\frac{\partial L(k)}{\partial a_i} = \frac{2\pi}{w_i} \sin\left(\frac{b_i k}{w_i} - \phi(k)\right) E_0, \quad (8)$$

$$\frac{\partial L(k)}{\partial w_i} = \left[\sin\left(\frac{b_i k}{w_i} - \phi(k)\right) \left(\frac{\pi^2 a_i k}{w_i^3} E_1 - \frac{2\pi a_i}{w_i^2} \right) - \frac{2\pi a_i b_i k}{w_i^3} \cos\left(\frac{b_i k}{w_i} - \phi(k)\right) \right] E_0, \quad (9)$$

$$\frac{\partial L(k)}{\partial b_i} = \frac{2\pi a_i b_i k}{w_i^2} \cos\left(\frac{b_i k}{w_i} - \phi(k)\right) E_0, \quad (10)$$

where

$$E_0 = \frac{\text{sgn}(w_i)A(k)}{\exp(\frac{\pi k}{2w_i}) - \exp(-\frac{\pi k}{2w_i})},$$

$$E_1 = \frac{\exp(\frac{\pi k}{2w_i}) + \exp(-\frac{\pi k}{2w_i})}{\exp(\frac{\pi k}{2w_i}) - \exp(-\frac{\pi k}{2w_i})}.$$

The descent increment at any direction, say, with respect to parameter Θ_{ij} , is

$$\frac{\partial L}{\partial \Theta_{ij}} = \int_{-\infty}^{+\infty} \frac{\partial L(k)}{\partial \Theta_{ij}} dk. \quad (11)$$

The absolute contribution from frequency k to this total amount at Θ_{ij} is

$$\left| \frac{\partial L(k)}{\partial \Theta_{ij}} \right| \approx A(k) \exp(-|\pi k / 2w_j|) G_{ij}(\Theta_i, k), \quad (12)$$

where $\Theta_i \triangleq \{w_i, b_i, a_i\}$, $\Theta_{ij} \in \Theta_i$, $G_{ij}(\Theta_i, k)$ is a function with respect to Θ_i and k , which can be found in one of Eqs. (8, 9, 10).

When the component at frequency k where $\hat{Y}(k)$ is not close enough to $\hat{f}(k)$, $\exp(-|\pi k / 2w_i|)$ would dominate $G_{ij}(\Theta_i, k)$ for a small w_i . Therefore, the behavior of Eq. (12) is dominated by $A(k) \exp(-|\pi k / 2w_i|)$. This dominant term also indicates that weights are much more important than bias terms, which will be verified by MNIST dataset in Appendix B.

Through the above framework of analysis, we have the following theorem (The proof can be found at Appendix C.) Define

$$W = (w_1, w_2, \dots, w_N)^T \in \mathbb{R}^N. \quad (13)$$

Theorem 1. Considering a DNN of one hidden layer with activation function $\sigma(x)$ being hyperbolic tangent, for any frequencies k_1 and k_2 such that $|\hat{f}(k_1)| > 0$, $|\hat{f}(k_2)| > 0$, and $|k_2| > |k_1| > 0$, there exist positive constants c and C such that for sufficiently small δ , we have

$$\frac{\mu\left(\left\{W : \left| \frac{\partial L(k_1)}{\partial \Theta_{ij}} \right| > \left| \frac{\partial L(k_2)}{\partial \Theta_{ij}} \right| \text{ for all } i, j\right\} \cap B_\delta\right)}{\mu(B_\delta)} \geq 1 - C \exp(-c/\delta), \quad (14)$$

where $B_\delta \subset \mathbb{R}^N$ is a ball with radius δ centered at the origin and $\mu(\cdot)$ is the Lebesgue measure.

Thm 1 indicates that for any two non-converged frequencies, with sufficiently small weights of DNN, the lower-frequency component of the loss function shall dominate over the higher frequencies during the gradient-based training. Specifically, with a sufficiently small initialization of DNN, our theorem demonstrates that the training process of DNN endows lower frequencies with a higher priority during the early stage of training. Through the proof of Thm 1, clearly, the decaying behavior of the Fourier transform of the transfer function is the key mechanism underlying the F-Principle. For large initial weights of DNN, because the decaying becomes slow, we may not be able to see a clear phenomenon of the F-Principle as observed in Fig. 5(c). As shown in Appendix D, the result of 2-d input and multiple hidden layers is qualitatively similar to the 1-d example in Fig. 5.

6. Conclusion and discussion

In this work, we empirically demonstrate that (i) the F-Principle is universal in the training process of DNNs; (ii) the F-Principle can provide insight into both the success and failure of DNNs; (iii) the F-Principle can be adopted to accelerate the convergence of low frequencies for scientific computing problems. As a first step towards a mathematical explanation of the F-Principle, we also prove a theorem for DNNs of one hidden layer. Now, it is still far from a complete theorem. However, it illustrates the key mechanism underlying the F-Principle—the activation function (including tanh and Relu) in the Fourier domain decays as frequency increases. Based on the same mechanism, our ongoing work provides a more rigorous mathematical study of the dynamical process of the loss function at different frequencies for general DNNs (e.g., DNNs of multiple hidden layers, different activation functions, high-dimensional inputs). To sum up, the F-Principle is ubiquitous, applicable, and explainable.

Next, we discuss DNN’s generalization ability. Traditional learning theory — which restricts capacity (such as VC dimension (Vapnik, 1999)) to achieve good generalization performance — cannot explain why DNNs with large capacity to memorize randomly labeled datasets (Cybenko, 1989) still possess good generalization ability for real datasets (Zhang et al., 2016). From the view point of Fourier analysis, our results on the F-Principle hint the following understanding of this result.

Denote sampling points of training dataset as $S_{train} = \{\mathbf{x}_i\}_{i=1}^N$. For a given training dataset, a sufficiently over-parameterized DNN is able to well fit the training data after training. Thus, the FT (Fourier transform) of the DNN out-

put estimated on S_{train} will always converge to the FT of the training data (even for the parity function where S_{train} takes a fraction of all possible inputs). Focusing on the FT on S_{train} , the F-Principle states that low-frequencies will converge first, later high-frequencies. The F-Principle implicates that, among all the functions that can fit the training data, a DNN is implicitly biased during the training towards a function with more power at low frequencies. This bias is important because of the following two reasons. First, for many real-world problems, this bias is consistent with the property of low-frequency dominance underlying many real datasets, e.g., MNIST/CIFAR10. Second, Fourier analysis measures how fast a function can change within a small neighborhood in its input domain, thus, provides a natural measure of complexity (Novak et al. (2018)). Therefore, this bias often leads to a DNN of low complexity function after training. Based on conventional wisdom, a low-complexity function usually has good generalization ability. Therefore, this implicit bias of the F-Principle provides a natural mechanism underlying the good generalization performance of DNNs often observed in practice.

However, if the size of the training dataset is small, components of frequencies higher than certain k of the true target function will be mostly aliased. Note that this k increases as the size of training data increases. Under this condition, based on the F-Principle, FT of DNN output on $S_{total} = S_{train} \cup S_{test}$ tends to concentrate on lower frequencies while compromising the frequencies higher than k . If the frequencies higher than k of true target function is negligible, then DNN can generalize well. Otherwise, we need to increase the size of training dataset.

In presence of noise, for a target function dominated by low frequencies, in general, high frequencies will be more severely contaminated due to their small amplitude. With early stopping, the F-Principle can prevent DNNs from fitting these noisy high frequencies to achieve a better generalization performance. For example, Neyshabur et al. (2014) shows that with five percent random labels on MNIST/CIFAR10, early-stopping can help achieve a better test accuracy.

References

- Arpit, D., Jastrzebski, S., Ballas, N., Krueger, D., Bengio, E., Kanwal, M. S., Maharaj, T., Fischer, A., Courville, A., Bengio, Y., et al. A closer look at memorization in deep networks. *arXiv preprint arXiv:1706.05394*, 2017.
- Bartlett, P. L. and Mendelson, S. Rademacher and gaussian complexities: Risk bounds and structural results. *Journal of Machine Learning Research*, 3(Nov):463–482, 2002.
- Bartlett, P. L., Maiorov, V., and Meir, R. Almost linear vc dimension bounds for piecewise polynomial networks. In

- Advances in Neural Information Processing Systems*, pp. 190–196, 1999.
- Bartlett, P. L., Foster, D. J., and Telgarsky, M. J. Spectrally-normalized margin bounds for neural networks. In *Advances in Neural Information Processing Systems*, pp. 6240–6249, 2017a.
- Bartlett, P. L., Harvey, N., Liaw, C., and Mehrabian, A. Nearly-tight vc-dimension and pseudodimension bounds for piecewise linear neural networks. *arXiv preprint arXiv:1703.02930*, 2017b.
- Bousquet, O. and Elisseeff, A. Stability and generalization. *Journal of machine learning research*, 2(Mar):499–526, 2002.
- Bracewell, R. N. and Bracewell, R. N. *The Fourier transform and its applications*, volume 31999. McGraw-Hill New York, 1986.
- Cybenko, G. Approximation by superpositions of a sigmoidal function. *Mathematics of control, signals and systems*, 2(4):303–314, 1989.
- Dinh, L., Pascanu, R., Bengio, S., and Bengio, Y. Sharp minima can generalize for deep nets. *arXiv preprint arXiv:1703.04933*, 2017.
- Dziugaite, G. K. and Roy, D. M. Computing nonvacuous generalization bounds for deep (stochastic) neural networks with many more parameters than training data. *arXiv preprint arXiv:1703.11008*, 2017.
- E, W. and Yu, B. The deep ritz method: A deep learning-based numerical algorithm for solving variational problems. *Communications in Mathematics and Statistics*, 6(1):1–12, 2018.
- E, W., Han, J., and Jentzen, A. Deep learning-based numerical methods for high-dimensional parabolic partial differential equations and backward stochastic differential equations. *Communications in Mathematics and Statistics*, 5(4):349–380, 2017.
- E, W., Ma, C., and Wu, L. A priori estimates of the generalization error for two-layer neural networks. *arXiv preprint arXiv:1810.06397*, 2018.
- Evans, L. C. *Partial differential equations*. 2010.
- Fan, Y., Lin, L., Ying, L., and Zepeda-Núñez, L. A multiscale neural network based on hierarchical matrices. *arXiv preprint arXiv:1807.01883*, 2018.
- Golowich, N., Rakhlin, A., and Shamir, O. Size-independent sample complexity of neural networks. *arXiv preprint arXiv:1712.06541*, 2017.
- Han, J., Zhang, L., Car, R., et al. Deep potential: A general representation of a many-body potential energy surface. *arXiv preprint arXiv:1707.01478*, 2017.
- Hardt, M., Recht, B., and Singer, Y. Train faster, generalize better: Stability of stochastic gradient descent. *arXiv preprint arXiv:1509.01240*, 2015.
- He, J., Li, L., Xu, J., and Zheng, C. Relu deep neural networks and linear finite elements. *arXiv preprint arXiv:1807.03973*, 2018.
- Hochreiter, S. and Schmidhuber, J. Simplifying neural nets by discovering flat minima. In *Advances in neural information processing systems*, pp. 529–536, 1995.
- Keskar, N. S., Mudigere, D., Nocedal, J., Smelyanskiy, M., and Tang, P. T. P. On large-batch training for deep learning: Generalization gap and sharp minima. *arXiv preprint arXiv:1609.04836*, 2016.
- Khoo, Y., Lu, J., and Ying, L. Solving parametric pde problems with artificial neural networks. *arXiv preprint arXiv:1707.03351*, 2017.
- Kingma, D. P. and Ba, J. Adam: A method for stochastic optimization. *arXiv preprint arXiv:1412.6980*, 2014.
- Krizhevsky, A., Nair, V., and Hinton, G. Cifar-10 (canadian institute for advanced research). URL <http://www.cs.toronto.edu/kriz/cifar.html>, 2010.
- LeCun, Y. The mnist database of handwritten digits. <http://yann.lecun.com/exdb/mnist/>, 1998.
- Neyshabur, B., Tomioka, R., and Srebro, N. In search of the real inductive bias: On the role of implicit regularization in deep learning. *arXiv preprint arXiv:1412.6614*, 2014.
- Neyshabur, B., Bhojanapalli, S., McAllester, D., and Srebro, N. Exploring generalization in deep learning. In *Advances in Neural Information Processing Systems*, pp. 5947–5956, 2017.
- Neyshabur, B., Li, Z., Bhojanapalli, S., LeCun, Y., and Srebro, N. Towards understanding the role of over-parametrization in generalization of neural networks. *arXiv preprint arXiv:1805.12076*, 2018.
- Novak, R., Bahri, Y., Abolafia, D. A., Pennington, J., and Sohl-Dickstein, J. Sensitivity and generalization in neural networks: an empirical study. *arXiv preprint arXiv:1802.08760*, 2018.
- Nye, M. and Saxe, A. Are efficient deep representations learnable? 2018.

- Poggio, T., Kawaguchi, K., Liao, Q., Miranda, B., Rosasco, L., Boix, X., Hidary, J., and Mhaskar, H. Theory of deep learning iii: the non-overfitting puzzle. Technical report, Technical report, CBMM memo 073, 2018.
- Rahaman, N., Arpit, D., Baratin, A., Draxler, F., Lin, M., Hamprecht, F. A., Bengio, Y., and Courville, A. On the spectral bias of deep neural networks. *arXiv preprint arXiv:1806.08734*, 2018.
- Shalev-Shwartz, S., Shamir, O., and Shammah, S. Failures of gradient-based deep learning. *arXiv preprint arXiv:1703.07950*, 2017.
- Soudry, D., Hoffer, E., Nacson, M. S., Gunasekar, S., and Srebro, N. The implicit bias of gradient descent on separable data. *Journal of Machine Learning Research*, 19(70), 2018.
- Vapnik, V. N. An overview of statistical learning theory. *IEEE transactions on neural networks*, 10(5):988–999, 1999.
- Wu, L., Zhu, Z., and E, W. Towards understanding generalization of deep learning: Perspective of loss landscapes. *arXiv preprint arXiv:1706.10239*, 2017.
- Xu, H. and Mannor, S. Robustness and generalization. *Machine learning*, 86(3):391–423, 2012.
- Xu, Z.-Q. J., Zhang, Y., and Xiao, Y. Training behavior of deep neural network in frequency domain. *arXiv preprint arXiv:1807.01251*, 2018.
- Zhang, C., Bengio, S., Hardt, M., Recht, B., and Vinyals, O. Understanding deep learning requires rethinking generalization. *arXiv preprint arXiv:1611.03530*, 2016.

A. Central difference scheme and Jacobi method

Consider a one-dimensional (1-d) Poisson's equation:

$$\begin{aligned} -\Delta u(x) &= g(x), \quad x \in \Omega = (-1, 1) \\ u(x) &= 0, \quad x = -1, 1. \end{aligned} \quad (15)$$

$[-1, 1]$ is uniformly discretized into $n + 1$ points with grid size $h = 2/n$. The Poisson's equation in Eq. (15) can be solved by the central difference scheme,

$$-\Delta u_i = -\frac{u_{i+1} - 2u_i + u_{i-1}}{(h)^2} = g(x_i), \quad i = 1, 2, \dots, n, \quad (16)$$

resulting a linear system

$$\mathbf{A}\mathbf{u} = \mathbf{g}, \quad (17)$$

where

$$A = \begin{pmatrix} 2 & -1 & 0 & 0 & \cdots & 0 \\ -1 & 2 & -1 & 0 & \cdots & 0 \\ 0 & -1 & 2 & -1 & \cdots & 0 \\ \vdots & \vdots & \cdots & & & \vdots \\ 0 & 0 & \cdots & 0 & -1 & 2 \end{pmatrix}_{(n-1) \times (n-1)}, \quad (18)$$

$$\mathbf{u} = \begin{pmatrix} u_1 \\ u_2 \\ \vdots \\ u_{n-2} \\ u_{n-1} \end{pmatrix}, \quad \mathbf{g} = (h)^2 \begin{pmatrix} g_1 \\ g_2 \\ \vdots \\ g_{n-2} \\ g_{n-1} \end{pmatrix}, \quad x_i = 2\frac{i}{n}. \quad (19)$$

A class of methods to solve this linear system is iterative schemes, for example, the Jacobi method. Let $A = D - L - U$, where D is the diagonal of A , and L and U are the strictly lower and upper triangular parts of $-A$, respectively. Then, we obtain

$$\mathbf{u} = D^{-1}(L + U)\mathbf{u} + D^{-1}\mathbf{g}. \quad (20)$$

The Jacobi iteration reads

$$\mathbf{u}^{l+1} = D^{-1}(L + U)\mathbf{u}^l + D^{-1}\mathbf{g}. \quad (21)$$

We perform the standard error analysis of the above iteration process. Denote \mathbf{u}^* as the true value obtained by directly performing inverse of A in Eq. (17). The error at step $l + 1$ is $\mathbf{e}^{l+1} = \mathbf{u}^{l+1} - \mathbf{u}^*$. Then, $\mathbf{e}^{l+1} = R_J \mathbf{e}^l$, where $R_J = D^{-1}(L + U)$. The converging speed of \mathbf{e}^l is determined by the eigenvalues of R_J , that is,

$$\lambda_k = \lambda_k(R_J) = \cos \frac{k\pi}{n}, \quad k = 1, 2, \dots, n-1, \quad (22)$$

and the corresponding eigenvector \mathbf{v}_k 's element is

$$\mathbf{v}_{k,j} = \sin \frac{jk\pi}{n}, \quad j = 1, 2, \dots, n-1. \quad (23)$$

So we can write

$$\mathbf{e}^l = \sum_{k=1}^{n-1} \alpha_k^l \mathbf{v}_k, \quad (24)$$

where α_k^l can be understood as the magnitude of \mathbf{e}^l in the direction of \mathbf{v}_k . Then,

$$\begin{aligned} \mathbf{e}^{l+1} &= \sum_{k=1}^{n-1} \alpha_k^l R_J \mathbf{v}_k = \sum_{k=1}^{n-1} \alpha_k^l \lambda_k \mathbf{v}_k. \\ \alpha_k^{l+1} &= \lambda_k \alpha_k^l. \end{aligned} \quad (25)$$

Therefore, the converging speed of \mathbf{e}^l in the direction of \mathbf{v}_k is controlled by λ_k . Since

$$\cos \frac{k\pi}{n} = -\cos \frac{(n-k)\pi}{n}, \quad (26)$$

the frequencies k and $(n-k)$ are closely related and converge with the same speed. Consider the frequency $k < n/2$, λ_k is larger for lower frequency. Therefore, lower frequency converges slower in the Jacobi method.

B. The effect of the norm of weight and bias terms

We use MNIST dataset to examine different effects between initial weights and initial bias terms. We use a Gaussian distribution with mean 0 to initialize DNN parameters. For simplicity, we use a *two-dimensional vector* (\cdot, \cdot) to denote standard deviations of weights and bias terms, respectively. Fix the standard deviation for bias terms, we consider the effect of different standard deviations of weights, that is, $(0.01, 0.01)$ in Fig. 6(a) and $(0.3, 0.01)$ in Fig. 6(b). As shown in Fig. 6, in both cases, DNNs have high accuracy for the training data. However, for the test data, the prediction accuracy of the small standard deviation (red dashed line in Fig. 6(a)) is much higher than that of the large one (yellow dashed line in Fig. 6(b)).

Note that the effect of initialization is governed by weights rather than bias terms. To verify this, we initialize bias terms with standard deviation 2.5. As shown by black curves in Fig. 6(a), the DNN with standard deviation $(0.01, 2.5)$ has a bit lower prediction accuracy.

C. Proof of theorem 1

Theorem. Consider a one hidden layer DNN with activation function $\sigma(x)$ being hyperbolic tangent. For any

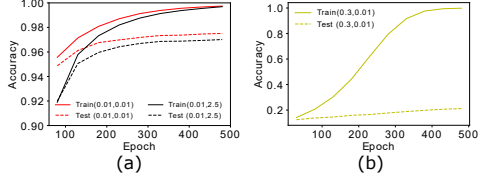


Figure 6. Analysis of the training process of DNNs with different initialization while fitting MNIST dataset. Illustrations are the prediction accuracy on the training data and the test data at different training epochs. We use a tanh-DNN with widths: 784-800-400-200-100-1. The learning rate is 10^{-5} with batch size 400. DNN parameters are initialized by Gaussian distribution with mean 0. The legend (\cdot, \cdot) denotes standard deviations of weights and bias terms, respectively. The DNN is trained by Adam optimizer (Kingma & Ba, 2014) with the MSE loss function.

frequencies k_1 and k_2 such that $|\hat{f}(k_1)| > 0$, $|\hat{f}(k_2)| > 0$, and $|k_2| > |k_1| > 0$, there exist positive constants c and C such that for sufficiently small δ , we have

$$\frac{\mu\left(\left\{W : \left|\frac{\partial L(k_1)}{\partial \Theta_{ij}}\right| > \left|\frac{\partial L(k_2)}{\partial \Theta_{ij}}\right| \text{ for all } i, j\right\} \cap B_\delta\right)}{\mu(B_\delta)} \geq 1 - C \exp(-c/\delta), \quad (27)$$

where $B_\delta \subset \mathbb{R}^N$ is a ball with radius δ centered at the origin and $\mu(\cdot)$ is the Lebesgue measure.

We remark that c and C depend on k_1 , k_2 , $|\hat{f}(k_1)|$, $|\hat{f}(k_2)|$, $\sup |a_i|$, $\sup |b_i|$, and N .

Proof. To prove the statement, it is sufficient to show that $\mu(S_{ij, \delta})/\mu(B_\delta) \leq C \exp(-c/\delta)$ for each i, j , where

$$S_{ij, \delta} := \left\{W \in B_\delta : \left|\frac{\partial L(k_1)}{\partial \Theta_{ij}}\right| \leq \left|\frac{\partial L(k_2)}{\partial \Theta_{ij}}\right|\right\}. \quad (28)$$

We prove this for $S_{i1, \delta}$, that is, $\Theta_{ij} = a_i$. The proofs for $\Theta_{ij} = w_i$ and b_i are similar. Without loss of generality, we assume that $k_1, k_2 > 0$, $b_i > 0$, and $w_i \neq 0$, $i = 1, \dots, N$. According to Eq. (8), the inequality $|\frac{\partial L(k_1)}{\partial a_i}| \leq |\frac{\partial L(k_2)}{\partial a_i}|$ is equivalent to

$$\frac{A(k_2)}{A(k_1)} \left| \frac{\exp(\frac{\pi k_1}{2w_i}) - \exp(-\frac{\pi k_1}{2w_i})}{\exp(\frac{\pi k_2}{2w_i}) - \exp(-\frac{\pi k_2}{2w_i})} \right| \cdot \left| \sin\left(\frac{b_i k_2}{w_i} - \phi(k_2)\right) \right| \geq \left| \sin\left(\frac{b_i k_1}{w_i} - \phi(k_1)\right) \right| \quad (29)$$

Note that $|\hat{\Upsilon}(k)| \leq C \sum_{i=1}^N \frac{|a_i|}{|w_i|} \exp(-\frac{\pi k}{2|w_i|})$ for $k > 0$. Thus

$$\lim_{W \rightarrow 0} \hat{\Upsilon}(k) = 0 \quad \text{and} \quad \lim_{W \rightarrow 0} D(k) = -\hat{f}(k). \quad (30)$$

Therefore,

$$\lim_{W \rightarrow 0} A(k) = |\hat{f}(k)| \quad \text{and} \quad \lim_{W \rightarrow 0} \phi(k) = \pi + \arg(\hat{f}(k)). \quad (31)$$

For $W \in B_\delta$ with sufficiently small δ , $A(k_1) > \frac{1}{2}|\hat{f}(k_1)| > 0$ and $A(k_2) < 2|\hat{f}(k_2)|$. Also note that $|\sin(\frac{b_i k_2}{w_i} - \phi(k_2))| \leq 1$ and that for sufficiently small δ ,

$$\left| \frac{\exp(\frac{\pi k_1}{2w_i}) - \exp(-\frac{\pi k_1}{2w_i})}{\exp(\frac{\pi k_2}{2w_i}) - \exp(-\frac{\pi k_2}{2w_i})} \right| \leq 2 \exp\left(\frac{-\pi(k_2 - k_1)}{2|w_i|}\right). \quad (32)$$

Thus, inequality (29) implies that

$$\left| \sin\left(\frac{b_i k_1}{w_i} - \phi(k_1)\right) \right| \leq \frac{8|\hat{f}(k_2)|}{|\hat{f}(k_1)|} \exp\left(-\frac{\pi(k_2 - k_1)}{2|w_i|}\right). \quad (33)$$

Noticing that $\frac{2}{\pi}|x| \leq |\sin(x)|$ ($|x| \leq \frac{\pi}{2}$) and Eq. (31), we have for $W \in S_{ij, \delta}$, for some $n \in \mathbb{Z}$,

$$\left| \frac{b_i k_1}{w_i} - \arg(\hat{f}(k_1)) - n\pi \right| \leq \frac{8\pi|\hat{f}(k_2)|}{|\hat{f}(k_1)|} \exp\left(-\frac{\pi(k_2 - k_1)}{2\delta}\right) \quad (34)$$

that is,

$$\begin{aligned} -c_1 \exp(-c_2/\delta) + n\pi + \arg(\hat{f}(k_1)) &\leq \frac{b_i k_1}{w_i} \\ &\leq c_1 \exp(-c_2/\delta) + n\pi + \arg(\hat{f}(k_1)), \end{aligned} \quad (35)$$

where $c_1 = \frac{8\pi|\hat{f}(k_2)|}{|\hat{f}(k_1)|}$ and $c_2 = \pi(k_2 - k_1)$. Define $I := I^+ \cup I^-$ where

$$I^+ := \{w_i > 0 : W \in S_{ij, \delta}\}, \quad I^- := \{w_i < 0 : W \in S_{ij, \delta}\}. \quad (36)$$

For $w_i > 0$, we have for some $n \in \mathbb{Z}$,

$$\begin{aligned} 0 &< \frac{b_i k_1}{c_1 \exp(-c_2/\delta) + n\pi + \arg(\hat{f}(k_1))} \leq w_i \\ &\leq \frac{b_i k_1}{-c_1 \exp(-c_2/\delta) + n\pi + \arg(\hat{f}(k_1))}. \end{aligned} \quad (37)$$

Since $W \in B_\delta$ and $c_1 \exp(-c_2/\delta) + \arg(\hat{f}(k_1)) \leq 2\pi$, we have $\frac{b_i k_1}{2\pi + n\pi} \leq w_i \leq \delta$. Then Eq. (37) only holds for some large n , more precisely, $n \geq n_0 := \frac{b_i k_1}{\pi \delta} - 2$. Thus we obtain the estimate for the (one-dimensional) Lebesgue measure of I^+

$$\begin{aligned} \mu(I^+) &\leq \sum_{n=n_0}^{\infty} \left| \frac{b_i k_1}{-c_1 \exp(-c_2/\delta) + n\pi + \arg(\hat{f}(k_1))} \right. \\ &\quad \left. - \frac{b_i k_1}{c_1 \exp(-c_2/\delta) + n\pi + \arg(\hat{f}(k_1))} \right| \\ &\leq 2|b_i|k_1 c_1 \exp(-c_2/\delta) \cdot \\ &\quad \sum_{n=n_0}^{\infty} \frac{1}{(n\pi + \arg(\hat{f}(k_1)))^2 - (c_1 \exp(-c_2/\delta))^2} \\ &\leq C \exp(-c/\delta). \end{aligned} \quad (38)$$

The similar estimate holds for $\mu(I^-)$, and hence $\mu(I) \leq C \exp(-c/\delta)$. For $W \in B_\delta$, the $(N-1)$ dimensional vector $(w_1, \dots, w_{i-1}, w_{i+1}, \dots, w_N)^T$ is in a ball with radius δ in \mathbb{R}^{N-1} . Therefore, we finally arrive at the desired estimate

$$\frac{\mu(S_{i1,\delta})}{\mu(B_\delta)} \leq \frac{\mu(I)\omega_{N-1}\delta^{N-1}}{\omega_N\delta^N} \leq C \exp(-c/\delta), \quad (39)$$

where ω_d is the volume of a unit ball in \mathbb{R}^d . □

D. Memorizing 2-d image

We train a DNN to fit a natural image (See Fig. 7(a)), a mapping from coordinate (x,y) to gray scale strength, where the latter is subtracted by its mean and then normalized by the maximal absolute value. First, we initialize DNN parameters by a Gaussian distribution with mean 0 and standard deviation 0.08 (initialization with small parameters). From the snapshots during the training process, we can see that the DNN captures the image from coarse-grained low frequencies to detailed high frequencies (Fig. 7(b)). As an illustration of the F-Principle, we study the Fourier transform of the image with respect to x for a fixed y (red dashed line in Fig. 7(a), denoted as the target function $f(x)$ in the spatial domain). The DNN can well capture this 1-d slice after training as shown in Fig. 7(c). Fig. 7(d) displays the amplitudes $|\hat{f}(k)|$ of the first 40 frequency components. Due to the small initial parameters, as an example in Fig. 7(d), when the DNN is fitting low-frequency components, high frequencies stay relatively small. As the relative error shown in Fig. 7(e), the first five frequency peaks converge from low to high in order.

Next, we initialize DNN parameters by a Gaussian distribution with mean 0 and standard deviation 1 (initialization with large parameters). After training, the DNN can well capture the training data, as shown in the left in Fig. 7(f). However, the DNN output at the test pixels are very noisy, as shown in the right in Fig. 7(f). For the pixels at the red dashed lines in Fig. 7(a), as shown in Fig. 7(g), the DNN output fluctuates a lot. Compared with the case of small initial parameters, as shown in Fig. 7(h), the convergence order of the first five frequency peaks do not have a clear order.

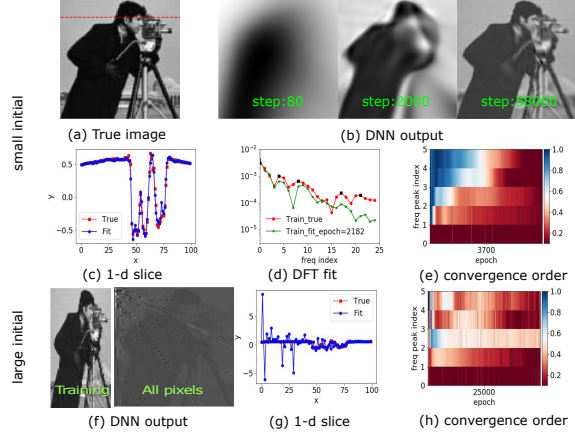


Figure 7. F-Principle in fitting a natural image. The training data are all pixels whose horizontal indices are odd. We initialize DNN parameters by a Gaussian distribution with mean 0 and standard deviation 0.08 (small initial) or 1 (large initial). (a) True image. (b-g) correspond to the case of the small initial parameters. (f-h) correspond to the case of the large initial parameters. (b) DNN outputs of all pixels at different training epochs. (c, g) DNN outputs (blue) and the true gray-scale (red) of test pixels at the red dashed position in (a). (d) $|\hat{Y}(k)|$ (green) at certain training epoch and $|\hat{f}(k)|$ (red) at the red dashed position in (a), as a function of frequency index. Selected peaks are marked by black dots. (e, h) $\Delta_F(k)$ computed by the training data at different epochs for the selected frequencies in (d). (f) DNN outputs of training pixels (left) and all pixels (right) after training. We use a tanh-DNN with widths 2-400-200-100-1. We train the DNN with the full batch and learning rate 0.0002. The DNN is trained by Adam optimizer (Kingma & Ba, 2014) with the MSE loss function.